Optica Applicata, Vol. XXXVI, No. 4, 2006

Spectral optical coherence tomography for nondestructive examinations

PIOTR TARGOWSKI[1], TOMASZ BAJRASZEWSKI[1], IWONA GORCZYŃSKA[1], MICHALINA GÓRA[1], ANNA SZKULMOWSKA[1], MACIEJ SZKULMOWSKI[1], MACIEJ WOJTKOWSKI[1], JAKUB J. KALUZNY[2], BARTLOMIEJ J. KALUZNY[2], ANDRZEJ KOWALCZYK[1]

[1]Institute of Physics, Nicolaus Copernicus University, Grudziądzka 5, 87-100 Toruń, Poland

[2]Department of Ophthalmology, Collegium Medicum, Nicolaus Copernicus University, M. Skłodowskiej-Curie 9, 85-094 Bydgoszcz, Poland

An overview of the spectral optical coherence tomography which is the alternative to the traditional Time domain version is given. Examples of applications in ophthalmology as well as in art preservation are presented.

Keywords: spectral optical coherence tomography, ophthalmic imaging, nondestructive testing.

1. Introduction

Spectral optical coherence tomography (SOCT) [1] compared to the classical time domain optical coherence tomography (TdOCT) [2] offers a better signal-to-noise ratio [3–5]. Additionally, this method permits one line of an image (an A-scan) to be collected at a time as short as 30 microseconds, thus 100 times faster than in TdOCT. The short data collection time dramatically reduces motion artifacts and leads to improvement of the image quality by increasing the line density. Furthermore, it opens space for new applications such as *in vivo* 3D imaging [6–10], tomographic movies [9] for investigation of microstructure dynamics of tissues and surfaces of oil paintings. It also expands the scale of measured phase differences, and consequently, increases the measurement range of velocities (*e.g.*, of blood flow in vessels [11, 12]) varying from 0.1 to 5 mm/s. Direct access to spectral data facilitates numerical dispersion correction and absorption measurements.

This contribution reviews the physical foundations of SOCT and its implementation. The paper presents examples of nondestructive examinations in ophthalmology as well as in the art conservation.

2. The method

In SOCT, the information on locations of structural elements (interfaces) within the object is encoded in the recorded spectrum and must be extracted with the aid of Fourier

transformation. Briefly, in SOCT a recorded signal $I_{\mathrm{tot}}(\omega)$ is a product of spectrum $S(\omega)$ of a light source and interference fringes. The signal from an object containing n back scattering interfaces can be expressed as follows:

$$I_{\mathrm{tot}}(\omega) = \\ = S(\omega)\left[\alpha_r + \sum_n \alpha_n + 2\sum_{n\neq m} \sqrt{\alpha_n\alpha_m}\cos(\omega\tau_{nm}) + 2\sum_n \sqrt{\alpha_n\alpha_r}\cos(\omega\tau_{nr})\right] \tag{1}$$

where $\tau_{nm} = \tau_n - \tau_m$ and $\tau_{nr} = \tau_n - \tau_r$. Symbols τ_n and τ_r denote propagation time of light scattered from the n-th interface in the object and light reflected from the reference mirror, respectively; α_r is the reflection coefficient of reference mirror, α_n describes the reflectivity of n-th interface within the object examined. The first two terms represent non-interference components of the signal. The terms containing α_r predominate since the intensity of light reflected from the reference mirror is made much higher than that returning from the object to achieve shot noise limited detection. The first term and other signals arising from interferences of light reflected from various surfaces inside the instrument (not shown in Eq. (1) for simplicity) are removed in the process of background subtraction. The background is registered once per measurement with the object being removed from the interferometer. The result of the subtraction undergoes the Fourier transformation, producing a set of Dirac's deltas δ convolved with $\Gamma(\tau)$ – the autocoherence function of the light source which is the Fourier transform of its spectrum $S(\omega)$:

$$|i(\tau)| = \mathrm{FT}(I(\omega)) = \\ = |\Gamma(\tau)| \otimes \left[\delta(\tau)\sum_n \alpha_n + \sum_{n\neq m} \sqrt{\alpha_n\alpha_m}\,\delta(\tau \pm \tau_{nm}) + \sum_n \sqrt{\alpha_n\alpha_r}\,\delta(\tau \pm \tau_{nr})\right] \tag{2}$$

The first term is always located at $\tau = 0$ and is easily recognized as a horizontal line in the tomogram. The second term arises from the interferences between waves backreflected within the object. They can be kept under shot noise because we can take advantage of coherent detection by adjusting $\alpha_r \gg \alpha_n, \alpha_m$ [13]. The third term carries the information about locations of the structural interfaces with respect to the position of the reference mirror. It must be noted that the modulus of the Fourier transform of the real valued function (the spectrum) is symmetrical. Therefore, each term located at $\tau = \tau_{mn}$ and $\tau = \tau_{nr}$ in Eq. (2) has its mirror image at $\tau = -\tau_{mn}$ and $\tau = -\tau_{nr}$.

If mirror images overlap (which happens in the case of thick objects) the phase stepping procedures and algorithms which remove one of the mirror images must be

adapted [14–17]. This is done at the cost of extending the measurement time by two to four times.

The major advantage of SOCT lies in the high acquisition speed, which is due not only to the lack of moving parts in the reference arm, but also to the high signal-to-noise ratio. The latter permits a short exposition time of the CCD, even for low irradiation of the object (the eye, a painting). It is possible to obtain high quality tomograms with a speed of 30000 A-scans per second even with irradiation level of 200 μW, which is especially important in the case of eye imaging [18].

It can be roughly estimated that SOCT systems are a hundred times faster than TdOCT. This advantage of speed is usually used to get A-scans of high density, with transversal scanner step much smaller than the lateral resolution (Fig. 2). Such over-sampled tomograms show increase in the sensitivity and quality [18, 19]. As a rule of thumb, collection of about 1000 A-scans per one millimeter of an image may be recommended. This procedure also increases the number of details visible by reducing the effective speckle size and improves the delineation of internal structure.

Another significant advantage of SOCT lies in dispersion correction. If a very broadband light source is used in OCT instrument to achieve high axial resolution, the quality of resulting tomograms is disappointingly spoiled by a dispersion broadening. This effect can be limited by a careful balance of dispersion in both arms of the interferometer, but usually cannot be completely eliminated, mostly due to the refraction in the object examined (vitreous in the eye, varnish and paint layer in the painting). In contrast to time domain, the SOCT offers additional ability of numerical correction during the post-processing of the image. This numerically effective and simple method is possible due to the availability of spectral information of interfering light [10].

3. The instrument

The tomograms shown in this paper were obtained with a home-made instrument based on an optical fiber Michelson interferometer set-up (Fig. 1). As a light source (LS), we use a tandem of superluminescence diodes (*Broadlighter* from Superlum, Russia) of a central wavelength $\lambda_{\text{centre}} = 823$ nm and spectral bandwidth $\Delta\lambda_{\text{FWHM}} = 74$ nm. The light of high spatial but low temporal coherence with output power of 3 mW is launched into one of the single mode fibers of the 50:50 fiber coupler DC through an optical isolator IO. The optical isolator protects the light source from the light back reflected from the elements of the interferometer. The light is split by the coupler into the reference and object arms. The former contains a polarization controller PCO and a collimator, and is terminated by a mirror RM kept in a fixed position. The object arm consists of a fiber connected to a collimator, transversal scanners X–Y and lenses L and L_1 which form the measuring head. The interface optics allows the imaging of either the retina (the pivot point of the scanner and the pupil of the eye are located at two conjugate planes of the system of two achromatic lenses – both with focal lengths of 30 mm, the collimated beam leaving this system is focused on the retina by the eye

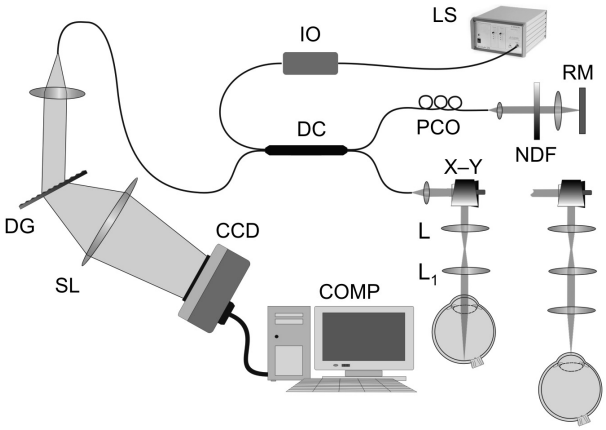

Fig. 1. Diagram of the instrument: LS – superluminescent light source, IO – fiber isolator, DC – directional fiber coupler, PCO – polarization controller, NDF – neutral density filter, RM – reference arm mirror, X–Y – galvoscanner, L_1, L – lenses, DG – diffraction grating, SL – spectrometer lens, CCD – line scan camera, COMP – personal computer.

lens) or the anterior part of the eye (additional achromatic lens with $f = 25.4$ mm is placed after the two achromatic doublets that focus the beam on a desired structure). The former arrangement is used to investigations of the art items. The narrow beam of light penetrates the object, scatters from the elements of its structure, then is collected by the same optics L and L_1 back to the coupler DC. Then it interferes with the light returning from the reference arm and the interference signal is analysed and registered by a spectrometer. It consists of a volume phase holographic grating DG with 1200 lines/mm and achromatic lens SL ($f = 150$ mm) which focuses the spectrum on a 12-bit line scan CCD camera. The spectral fringe patterns registered by this detector are then transferred to a personal computer COMP. The resulting signal is Fourier transformed into an A-scan.

The system operates in the shot noise limited detection mode (the intensity of light in the reference arm of interferometer is controlled by neutral density filter NDF) with sensitivity of 90 dB. The exposure time per A-scan is usually equal to 42 μs.

The axial resolution of the system (equals to the coherence length of the light) is 4 μm in the medium with a refractive index ranging from 1.3 to 1.5. The transversal resolution is determined by the dimension of a light spot and depends on the aperture and aberration of the beam forming objective. In the case of the retina examination the optical system of the eye forms a light spot amounting to approximately 20 micrometers. In the case of corneal and art conservation imaging the transversal resolution is below 10 μm. In order to obtain either 2D slice (B-scan) or 3D volume tomogram the beam is scanned transversally by galvanometric scanners X–Y.

The signal is visualized in real time as a cross-sectional view and stored for post-processing. The numerical processing of the data, despite of the fast Fourier transformation, essential to the SOCT method, includes: subtraction of non-interference

background, spectral shaping [20] and numerical dispersion correction [10]. If necessary, in the case of 3D imaging, individual B-scans are automatically aligned to compensate for involuntary movements of the eye.

The eye examinations were performed at the eye clinic of the University Hospital following permission from the Ethic Committee. The optical power at the eye was kept at the level of about 700 μW, below the ANSI safety standard [21].

4. Results

4.1. Retinal imaging

In Figure 2, cross-sectional images of the same human retina, obtained with different lateral scanning density, but with the same axial resolution, are presented. In panel **a**, the scanning step is equal to the lateral resolution. In panel **b**, the same retina is scanned with oversampling. Increasing the density of scanning significantly improves the image quality and thus its diagnostic applicability. The examination time (0.3 s) is still short enough to eliminate artifacts caused by involuntary movements of the eye.

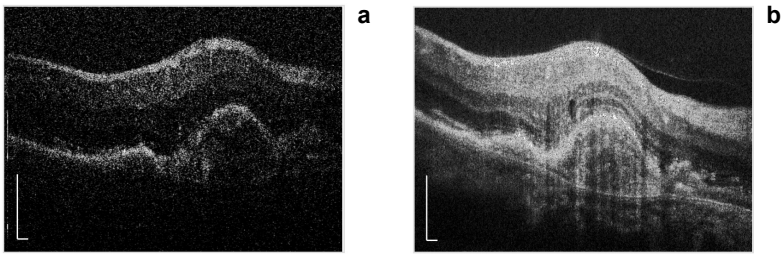

Fig. 2. Cross-sectional images of a human retina obtained with SOCT instrument. The bars indicate 200 μm in both directions: an image obtained with the scanner step equal to 15 μm, examination time equal to 0.02 s (**a**); the same retina scanned with the step of 1 μm, examination time equal to 0.3 s (**b**). Only in panel **b** posterior face of vitreous body indicating its partial detachment is visible.

High speed of SOCT allows real time imaging or recording of tomographic movies showing functional properties of the tissue examined such as blood vessel pulsations [9]. It also permits a 3D imaging (Fig. 3) in examination time acceptable for a patient. In this case both transversal scanners X–Y (Fig. 1) are utilized: one of the scanners moves slowly to collect a set of B-scans; each of these is obtained by fast sweep of the second scanner. As a result a "flow trough" tomographic movies can be generated as a new aid for medical diagnosis. If the 3D data set is recorded with sufficient density of B-scans, other cross-sections in directions different from those originally recorded may be generated. Moreover, by simply adding all intensities over whole A-scans, the fundus camera-like image can be generated:

$$I_{\text{image}} = \sum_{\tau} |i(\tau)| \tag{3}$$

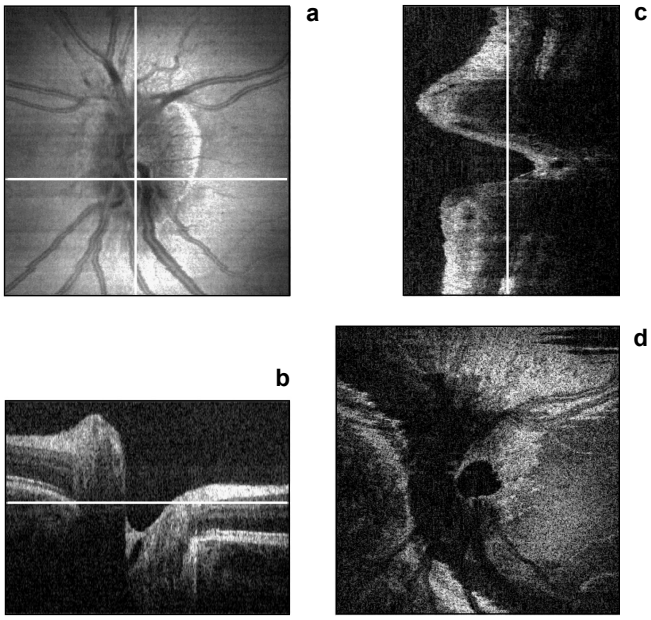

Fig. 3. Images of an optical disc from a healthy human retina obtained from 3D data: fundus camera-like view, lines indicate positions of cross-sectional views (**a**); **b**) one of the B-scans collected during sequential examination (**b**); B-scan constructed from 3D data in direction perpendicular to fast scanning (**c**); en-face tomogram constructed from 3D data at the depth indicated by lines in panels **b** and **c** (**d**). To generate these images a set of 385×385 A-scans was collected in 6 seconds.

The image (Fig. 3**a**) obtained with the aid of Eq. (3) permits the OCT tomogram to be precisely correlated with a fundus view, which ophthalmologists are used to examine.

The fast 3D imaging offers the possibility to create thickness maps of certain retinal layers and topographic visualization of chosen surfaces.

4.2. Anterior chamber imaging

SOCT technique may be considered as a valuable tool for the diagnostics of many pathologies or treatments as well as for assessing the contact lens fit (Fig. 4) [19].

However, there are some significant differences in application of SOCT to anterior chamber imaging. Firstly, SOCT image of the whole anterior chamber, as a thick structure, suffers from mirror image overlapping. This disadvantage can be overcome with the aid of one of many known methods [14–17], which unfortunately usually increases the examination time. In clinical practice, however, imaging of the whole chamber is quite rare and for visualization of pathologies a usual 2 mm thickness of OCT tomogram is sufficient (Fig. 5). Secondly, high imaging dynamics is necessary since the anterior chamber components, such as cornea are transparent, and quite often pathological changes are visible as distortions to fine, ordered structures of cornea only (Fig. 4). Surprisingly, visualization of cornea pathologies demands both

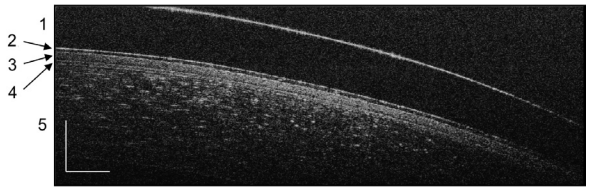

Fig. 4. An SOCT image of the cornea fitted with a hard contact lens: 1 – a contact lens, 2 – tear film, 3 – epithelium, 4 – Bowman's layer, 5 – stroma. Bars indicate 300 μm in both directions.

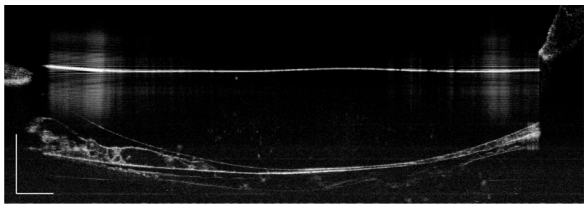

Fig. 5. An SOCT image of artificial inntraocular lens and posterior capsule opacificacton. Bars indicate 500 μm in both directions. The edges of the iris are visible at both sides of the lens. In proximity mirror reflexes from the lens surface, perpendicular to the beam, are evident.

better resolution and imaging dynamics than it is necessary for the retina. It is worthwhile to note that these demands are easier to fulfil with the aid of SOCT. Also, due to the high refraction at all interfaces in this area (air–cornea, air–contact lens, contact lens–cornea, cornea–aqueous humour, *etc.*) a refraction index correction by ray tracing is very often necessary to properly reveal the geometry [19].

4.3. Art conservation

Optical coherence tomography is recognised as a valuable tool also for non-invasive investigations of museum objects [22, 23]. Among others, there are several problems in art conservation where precise distance measurements are necessary. One of them is determination of varnish thickness. Knowledge of the thickness and structure of varnish layers is important both for conservation and for historical reasons. It is desirable to use non-invasive and non-contact techniques for this task in order to be able to apply it as often as necessary anywhere in the picture, including the sensitive region of the artist's signature. This technique would also make it possible to continuously monitor *in situ* the removal of varnish with laser ablation.

In Figure 6, an example of a 2D slice obtained with SOCT is presented and compared with microscopic image of the cross-section of a sample taken nearby.

The direct microscopic analysis of cross-section (Fig. 6**b**) obtained from the same picture indicates the presence of about 70 μm thick varnish layer. The same thickness is obtained from OCT measurement. The chemical assay indicates the oil-and-resin varnish, not tinted.

Since both interfaces are clearly resolvable, as one can see from Fig. 6**a**, an automatic procedure may be applied to detect their positions. A simple algorithm is based on

the assumption that both interfaces are continuous and well separated. The analysis is performed for every A-scan separately in two steps. Firstly, a first surface is recognised by convolution of A-scan intensity function with a narrow Gauss-shape function over the whole imaging depth. A position of the first maximum of a function thus obtained defines the first (air–vanish) interface. Then the image of this surface is erased from the original A-scan and a recognition procedure is repeated. The present first maximum then defines the second interface (varnish–paint) of the original image.

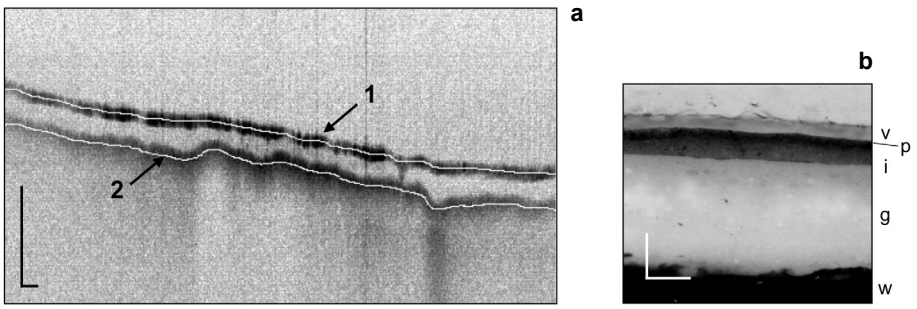

Fig. 6. An SOCT image of a cross-section of painting layer covered by varnish. The dark bands correspond to strong light scattering at the air–varnish (1) and varnish–paint layer (2) interfaces. The light penetrates from the top, the structures below the varnish layer are not visible due to high absorption of paint. White lines superimposed on interfaces indicate their positions as revealed by automatic structure recognition procedure (**a**). The microscopic image of the cross-section of a sample taken from the same object. The following layers are visible: v – varnish, p – paint layer, i – imprimitura, g – ground, w – wood (**b**). Bars indicates 200 μm in both images.

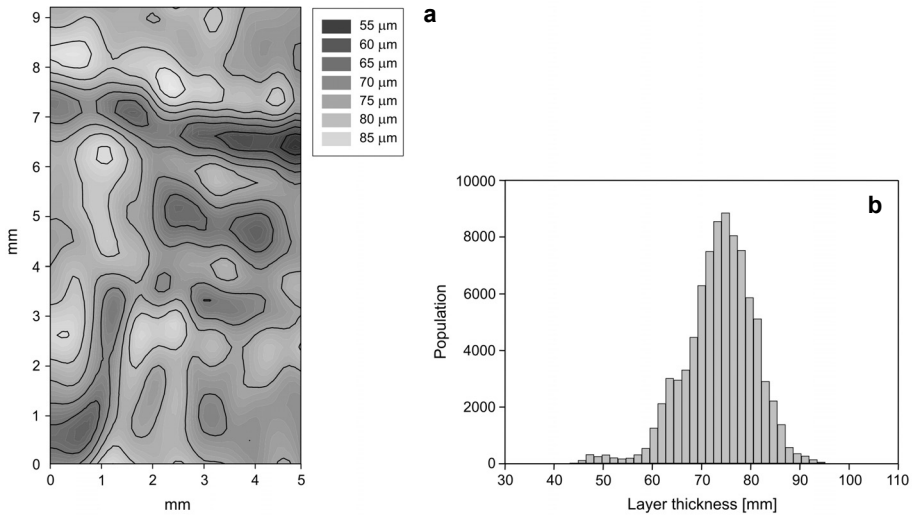

Fig. 7. Map of varnish layer thickness obtained by point-to-point subtraction of position of the air–varnish and varnish–paint layer interfaces (white lines in Fig. 6**a**) – **a**. A histogram of the varnish layer thickness – **b**.

Finally, the interfaces obtained are smoothed with a median filter. An exemplary result is shown in Fig. 6**a** as white lines superimposed on the OCT image.

The above procedure may be applied to a set of parallel B-scans and surface topography may thus be obtained. A point-to-point subtraction of both interface positions gives a varnish layer thickness map (Fig. 7**a**). This kind of data may be useful in planning varnish layer removal, for instance, by laser ablation.

Another problem is investigation of surface deformations of oil paintings on canvas during exposure to periodic changes of temperature and air humidity. These deformations of canvas support may lead to progressive destruction of the paint layer. The knowledge of the range and dynamics of these processes is important for preservation of artworks. Therefore, there is a need for precise profilometry of the painting surface.

In Figure 8**a,** a perspective view of surface profile (near the crack) of the sample of oil painting on linen canvas is presented. The surface profile recovering algorithm is similar to that used for the data shown in Fig. 7, but only the first air–paint interface is taken into account. Since the profile is given in digital form, a cross-section in any arbitrary plane may also be extracted (Fig. 8**b**). Similar data may be obtained in altered environmental conditions, for example, after a humidity jump and directly compared

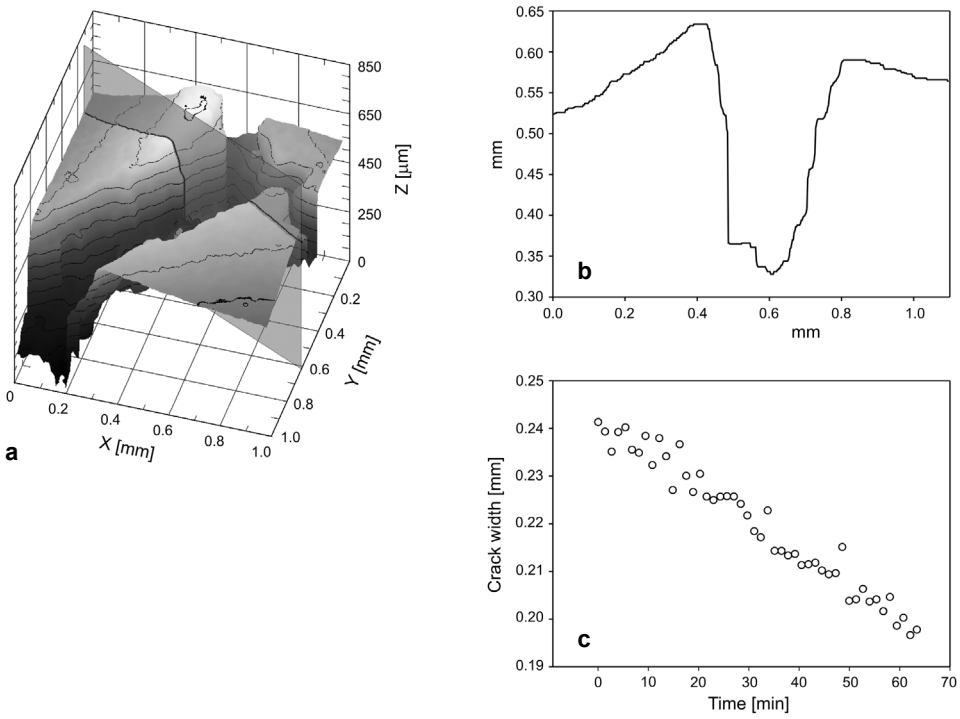

Fig. 8. A cracked paint surface reconstructed from the OCT data where the plane where the cross-section is extracted is also shown (**a**); a profile of the crack obtained in the cross-section plane (**b**); changes of the crack width caused by a surrounding humidity jump to 100 RH (**c**).

with the initial one. This kind of study may be performed *in situ* or in a laboratory, using a climate chamber. Because the method is fast, it is also possible to trace changes of the surface shape as a function of time after humidification or other environmental changes. As an investigated parameter the width of the crack at its half-depth is chosen (Fig. 8**c**).

5. Conclusions

The latest achievements in SOCT made this technique very useful for nondestructive examination. Major applications of SOCT are found in ophthalmology due to short data acquisition. It allows image quality to be increased by over-sampling and by decreasing image distortions due to involuntary movements of the patient's eye. It makes it possible to collect 3D data in reasonable time which may be further visualized by a different sophisticated method.

In art preservation SOCT offers the possibility of fast determination of varnish thickness and helps in tracing deformations which are relatively small and tend to develop during a long period of time. In contrast to other methods SOCT is insensitive to the displacements of the whole object between the sequential images. Additionally, it is fast enough to record the surface profile in seconds, to ensure that the image will represent a snap-shot, not blurred by changes in object structure during the data acquisition.

Acknowledgements – The support from the grant of the Polish Ministry of Science No. 2 H01E 025 25 is gratefully acknowledged.

References

[1] FERCHER A.F., *Optical coherence tomography*, Journal of Biomedical Optics **1**(2), 1996, pp. 157–73.
[2] HUANG D., SWANSON E.A., LIN C.P., SCHUMAN J.S., STINSON W.G., CHANG W., HEE M.R., FLOTTE T., GREGORY K., PULIAFITO C.A., FUJIMOTO J.G., *Optical coherence tomography*, Science **254**(5035), 1991, pp. 1178–81.
[3] CHOMA M.A., SARUNIC M.V, YANG C., IZATT J.A, *Sensitivity advantage of swept source and Fourier domain optical coherence tomography*, Optics Express **11**(18), 2003, pp. 2183–9.
[4] DE BOER J.F., CENSE B., PARK B.H., PIERCE M.C., TEARNEY G.J., BOUMA B., *Improved signal-to-noise ratio in spectral-domain compared with time-domain optical coherence tomography*, Optics Letters **28**(21), 2003, pp. 2067–9.
[5] LEITGEB R., HITZENBERGER C., FERCHER A., *Performance of fourier domain vs. time domain optical coherence tomography*, Optics Express **11**(8), 2003, pp. 889–94.
[6] PODOLEANU A.GH., ROGERS J.A., JACKSON D.A., DUNNE S., *Three dimensional OCT images from retina and skin*, Optics Express **7**(9), 2000, pp. 292–8.
[7] HITZENBERGER C.K., TROST P., LO P-W., ZHOU Q., *Three-dimensional imaging of the human retina by high-speed optical coherence tomography*, Optics Express **11**(21), 2003, pp. 2753–61.
[8] WOJTKOWSKI M., BAJRASZEWSKI T., GORCZYŃSKA I., TARGOWSKI P., KOWALCZYK A., WASIELEWSKI W., RADZEWICZ C., *Ophthalmic imaging by spectral optical coherence tomography*, American Journal of Ophthalmology **138**(3), 2004, pp. 412–9.

[9] WOJTKOWSKI M., SRINIVASAN V.J., KO T.H., FUJIMOTO J.G., KOWALCZYK A., DUKER J.S., *Ultrahigh -resolution, high-speed, Fourier domain optical coherence tomography and methods for dispersion compensation*, Optics Express **12**(11), 2004, pp. 2404–22.

[10] CENSE B., NASSIF N.A., CHEN T.C., PIERCE M.C., YUN S-H., PARK B.H., BOUMA B.E., TEARNEY G.J., DE BOER J.F., *Ultrahigh-resolution high-speed retinal imaging using spectral-domain optical coherence tomography*, Optics Express **12**(11), 2004, pp. 2435–47.

[11] LEITGEB R.A., SCHMETTERER L., DREXLER W., FERCHER A.F., ZAWADZKI R.J., BAJRASZEWSKI T., *Real -time assessment of retinal blood flow with ultrafast acquisition by color Doppler Fourier domain optical coherence tomography*, Optics Express **11**(23), 2003, pp. 3116–21.

[12] WHITE B.R., PIERCE M.C., NASSIF N., CENSE B., PARK B.H., TEARNEY G.J., BOUMA B.E., CHEN T.C., DE BOER J.F., *In vivo dynamic human retinal blood flow imaging using ultra-high-speed spectral domain optical Doppler tomography*, Optics Express **11**(25), 2003, pp. 3490–7.

[13] SZKULMOWSKA A., WOJTKOWSKI M., GORCZYŃSKA I., BAJRASZEWSKI T., SZKULMOWSKI M., TARGOWSKI P., KOWALCZYK A., KAŁUŻNY J.J., *Coherent noise-free ophthalmic imaging by spectral optical coherence tomography*, Journal of Physics D: Applied Physics **38**(15), 2005, pp. 2606–11.

[14] WOJTKOWSKI M., KOWALCZYK A., LEITGEB R., FERCHER A.F., *Full range complex spectral optical coherence tomography technique in eye imaging*, Optics Letters **27**(16), 2002, pp. 1415–7 .

[15] CHOMA M.A., YANG C., IZATT J.A., *Instantaneous quadrature low-coherence interferometry with 3×3 fiber-optic couplers*, Optics Letters **28**(22), 2003, pp. 2162–4.

[16] YASUNO Y., MAKITA S., ENDO T., AOKI G., SUMIMURA H., ITOH M., YATAGI T., *One-shot-phase-shifting Fourier domain optical coherence tomography by reference wavefront tilting*, Optics Express **12**(25), 2004, pp. 6184–91.

[17] TARGOWSKI P., GORCZYŃSKA I., SZKULMOWSKI M., WOJTKOWSKI M., KOWALCZYK A., *Improved complex spectral domain OCT for in vivo eye imaging*, Optics Communications **249**(1–3), 2005, pp. 357–62.

[18] SZKULMOWSKA A., GORCZYŃSKA I., BAJRASZEWSKI T., KOWALCZYK A., KAŁUŻNY J., WOJTKOWSKI M., FUJIMOTO J., *The applicability of standard resolution spectral optical coherence tomography for examination of the eye pathologies*, Proceedings of SPIE **5690**, 2005, pp. 85–90.

[19] SZKULMOWSKA A., GORCZYŃSKA I., SZKULMOWSKI M., TARGOWSKI P., KOWALCZYK A., KAŁUŻNY B.J., *High resolution spectral optical coherence tomography for clinical imaging of the anterior segment of the eye*, Proceedings of SPIE **5861**, 2005, pp. 586101-1–6.

[20] SZKULMOWSKI M., WOJTKOWSKI M., TARGOWSKI P., KOWALCZYK A., *Spectral shaping and least square iterative deconvolution in spectral OCT*, Proceedings of SPIE **5316**, 2004, pp. 424–31.

[21] *American National Standard for Safe Use of Lasers,* American National Standards Institute, ANSI Z 136.1, Orlando 2000.

[22] TARGOWSKI P., ROUBA B., WOJTKOWSKI M., KOWALCZYK A., *Application of optical coherence tomography to non-destructive examination of museum objects*, Studies in Conservation **49**(2), 2004, pp. 107–14.

[22] LIANG H., CID M.G., CUCU R.G., DOBRE G.M., PODOLEANU A.G., PEDRO J., SAUNDERS D., *En-face optical coherence tomography – a novel application of non-invasive imaging to art conservation*, Optics Express **13**(16), 2005, pp. 6133–44.

Received January 30, 2006